



This is a repository copy of *Morphological wavelet domain image watermarking*.

White Rose Research Online URL for this paper:  
<http://eprints.whiterose.ac.uk/75658/>

---

### Proceedings Paper:

Bhowmik, D. and Abhayaratne, C. (2007) Morphological wavelet domain image watermarking. In: 15th European Signal Processing Conference (EUSIPCO 2007). EUSIPCO 2007, 3-7 September 2007, Poznan, Poland. EURASIP , Poznan, Poland , pp. 2539-2543. ISBN 978-83-921340-2-2

---

### Reuse

Unless indicated otherwise, fulltext items are protected by copyright with all rights reserved. The copyright exception in section 29 of the Copyright, Designs and Patents Act 1988 allows the making of a single copy solely for the purpose of non-commercial research or private study within the limits of fair dealing. The publisher or other rights-holder may allow further reproduction and re-use of this version - refer to the White Rose Research Online record for this item. Where records identify the publisher as the copyright holder, users can verify any specific terms of use on the publisher's website.

### Takedown

If you consider content in White Rose Research Online to be in breach of UK law, please notify us by emailing [eprints@whiterose.ac.uk](mailto:eprints@whiterose.ac.uk) including the URL of the record and the reason for the withdrawal request.

# MORPHOLOGICAL WAVELET DOMAIN WATERMARKING

*D. Bhowmik and G. C. K. Abhayaratne*

Department of Electronic and Electrical Engineering, University of Sheffield  
Sheffield S1 3JD, United Kingdom.  
{d.bhowmik, c.abhayaratne}@sheffield.ac.uk

## ABSTRACT

Current digital watermarking methods based on the discrete wavelet transform use orthogonal wavelet kernels. In this paper, we discuss the use of morphological wavelets, which are a class of non-linear wavelets, in digital watermarking for scalable coded images. Three different scenarios for embedding the watermark, namely, 1) embedding only in the low pass subband (low-low), 2) embedding only in the high pass subbands (low-high, high-low and high-high) and 3) embedding in all subbands are considered to model popular wavelet domain watermarking methods. The performance of morphological Haar and higher length median wavelets in terms of embedding and detection under content adaptation attacks, such as resolution and quality scalable decoding are shown. Morphological wavelets based watermarking shows a high robustness against the content adaptation attacks, especially in resolution scalability, compared to the conventional orthogonal wavelets based watermarking.

## 1. INTRODUCTION

Digital watermarking is commonly used in content protection and authentication applications by means of hiding data that is used for verification in digital multimedia content. In digital watermarking for images, the watermark can be embedded on pixel domain or on frequency domain, which is usually realized by using a 2D transforms. The discrete wavelet transform (DWT) provides an intrinsic framework for multi resolution analysis of signals. Due to this reason and its ability to compact energy into a small number of coefficients, past years have seen the emergence of the wavelet transform domain watermarking algorithms [1]-[9]. They have shown great improvements in data capacity and high imperceptibility compared to the previous watermark embedding techniques [10]. Due to the fact that the DWT is widely used in image compression, wavelet based watermarking enables joint watermarking and compression by addressing a common framework [1, 7].

In all previously reported methods, only linear wavelet kernels have been used in watermark embedding and detection in wavelet domain. In particular, Most algorithms used orthogonal transforms, such as, Haar or Daubechies length-4 (D4) wavelet kernels. Recently, there have been watermarking examples on extending the choice of transform into M-band wavelets [8] and multi-wavelets [9]. Since the introduction of the lifting factorization [11] of the DWT, which provides a flexible framework to design non-linear wavelet transforms, non-linear wavelets have been used in image denoising and compression applications [12, 13, 14]. In the class of non-linear wavelets known as morphological wavelets, the linear lifting operators have been replaced by morphological operators [15, 16, 17].

An important requirement of digital image watermarking is that the watermark has to be robust to attacks, such as, adding noise, compression and content adaptation operations. With the emergence of scalable coding algorithms [18], the multimedia consumption chain uses scalable coded content in order to cater a wide range of usage requirements, such as various resolutions and bit rates. Images are usually encoded at full resolution at high quality, then the bit streams are adapted to create new bitstreams according to the required quality and resolution to cater channel bandwidths and display terminal resolutions. As such adaptations are becoming more and more common, partly due to the availability of scalable coding and partly due to modern operational requirements, it is vital that the embedded watermarking can be detected in the adapted contents, thereby high robustness against content adaptation attacks. Such robustness is dependent on which subbands are used in embedding the watermark, the method of embedding and the choice of wavelet transform kernel.

In this paper, we focus on the use of morphological wavelets in improving the robustness of watermarking against the content adaptation attacks. In section 2, we briefly describe how to design the morphological wavelets. We discuss the watermark embedding in wavelet domain in section 3. We show both embedding and robustness performance of morphological wavelets based watermarking and compare with those of orthogonal wavelets based watermarking in section 4 followed by the concluding remarks in section 5.

---

Mr. Bhowmik would like to thank EPSRC for the EPSRC-BP Dorothy Hodgkin Postgraduate Award (DHPA) during the performance of this work

## 2. MORPHOLOGICAL WAVELETS

The DWT is usually realized using filter banks. Every FIR filter bank can be decomposed into lifting steps by factoring its polyphase matrix using the Euclidean factoring algorithm [11]. Non-linear wavelets are obtained by replacing the linear operations, such as weighted averaging, in lifting steps with non-linear operations. They can modify only the lifting step(s) affecting the low pass sub band (known as update step) [15], only the lifting step(s) affecting the high pass subbands (known as prediction step) [16] and the both types of lifting steps [17]. We show the design steps for two morphological wavelet transforms: Morphological Haar (M-Haar) and Median lifting on quincunx sampling (M-QC).

### 2.1. Morphological Haar

Since non-linearities are introduced in the scaling function, we design the Morphological Haar based on the 2D non-separable decomposition. We start with a 2D input signal  $a^0$  with samples  $a_{m,n}^0$ , where  $m$  and  $n$  correspond to sampling indices, and its four 2D polyphase components  $(a, b, c, d)$ , mapped by an invertible splitting operator  $S^2$ , i.e.  $(a, b, c, d) = S^2(a^0)$ . The operator  $S^2$  forms a  $\begin{pmatrix} 2 & 0 \\ 0 & 2 \end{pmatrix}$  sampling matrix and invertible mapping, called the lazy wavelet, as follows:

$$\begin{aligned} a_{m,n} &= a_{2m,2n}^0, & b_{m,n} &= a_{2m+1,2n}^0, \\ c_{m,n} &= a_{2m,2n+1}^0 & \text{and } d_{m,n} &= a_{2m+1,2n+1}^0. \end{aligned} \quad (1)$$

We denote samples  $a_{m,n}$ ,  $b_{m,n}$ ,  $c_{m,n}$  and  $d_{m,n}$  by  $a$ ,  $b$ ,  $c$  and  $d$ , respectively. The lazy wavelet is lifted to 2-D Haar using  $P_3, P_2, P_1, U$  lifting as follows to obtain output subbands,  $a'$ ,  $b'$ ,  $c'$  and  $d'$ .

$$P_3 : \quad d' = \frac{1}{2}(d - (c + b - a)). \quad (2)$$

$$P_2 : \quad c' = c - (a - d'). \quad (3)$$

$$P_1 : \quad b' = b - (a - d'). \quad (4)$$

$$\begin{aligned} U : \quad a' &= \frac{1}{2}(a + b + c + d) \\ &= \frac{1}{2}(4a + (a - a) + (b - a) + (c - a) + (d - a)). \end{aligned} \quad (5)$$

It can be shown that,  $b - a = b' - d'$ ,  $c - a = c' - d'$  and  $d - a = b' + c'$ . Hence we can rewrite the final update step as

$$\begin{aligned} U : \quad a' &= 2a + \frac{1}{2}(0 + (b' - d') + (c' - d') + (b' + c')) \\ &= 2[a + \frac{1}{4}(0 + (b' - d') + (c' - d') + (b' + c'))] \\ &= 2[a + \text{mean}(0, (b' - d'), (c' - d'), (b' + c'))]. \end{aligned} \quad (6)$$

We replace the mean operator with the median operator to obtain the 2D morphological wavelet transform as

$$a + \text{median}(0, (b' - d'), (c' - d'), (b' + c')) = \text{median}(a, b, c, d). \quad (7)$$

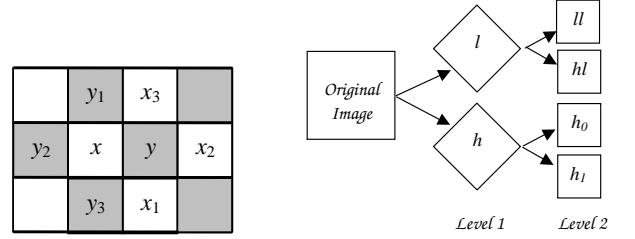


**Fig. 1.** Quincunx sampling: *Left:* Entries for prediction and update lifting steps, *Right:* Subbands after two levels of decomposition

The median operator, denoted by  $\text{median}(a, b, c, d)$ , returns the median of the values  $a, b, c, d$ , i.e., it takes the average of the two intermediate values. Thus if  $a \leq b \leq c \leq d$  then the median equals  $(b+c)/2$ . The inverse transform is obtained by reversing the order of operation and the operator of the lifting steps  $P_3 P_2 P_1 U$ .

### 2.2. Median lifting on quincunx sampling

We design 2D non-separable wavelet transforms by using the quincunx sampling lattice with the corresponding sampling matrix  $D = \begin{pmatrix} 1 & 1 \\ 1 & -1 \end{pmatrix}$ . Its determinant is 2 and thereby results in two polyphase components of the 2D signal each having dimensions equal to  $1/\sqrt{2}$  of the original signal dimensions. In the sequel we use  $\begin{pmatrix} m \\ n \end{pmatrix} = D \begin{pmatrix} i \\ j \end{pmatrix}$ , that is  $m = i + j$  and  $n = i - j$ . The splitting step for the 2D input signal  $a^0$  with samples  $a_{m,n}^0$  is given by

$$x_{i,j} = a_{m,n}^0 \text{ and } y_{i,j} = a_{m+1,n}^0. \quad (8)$$

We denote sample  $x_{i,j}$  by  $x$  and  $y_{i,j}$  by  $y$  and we refer to their respective neighbours as  $x_1, x_2, x_3$  and  $y_1, y_2, y_3$  as shown in Fig. 1. The white and gray boxes represent samples from  $x$  and  $y$  polyphase components, respectively. In this paper we are concerned with lifting steps of the form:

$$\text{Prediction : } y' = y - \text{median}(x, x_1, x_2, x_3), \quad (9)$$

$$\text{Update : } x' = x + \frac{1}{2} \text{median}(y', y'_1, y'_2, y'_3). \quad (10)$$

As mentioned earlier, one level of decompositions results in two subimages whose dimensions are reduced by  $\sqrt{2}$ . The transform steps are repeated on the low pass subimage ( $L$ ). In order to comply with the four subband structure, the high pass subimage ( $H$ ) in every odd numbered decomposition level is further decomposed into two subimages whose dimensions are reduced by a factor 2 after two decompositions. Consequently, after every even numbered decomposition every image is decomposed into four subimages with three details and one approximation image. By sticking to even number of decompositions, the resulting coefficients can be coded using

existing quantisation and entropy coding methods designed for separable four subband decomposition schemes. The right column of Fig. 1 shows the subimages after two levels of decompositions.

### 3. WAVELET BASED WATERMARKING

We categorize wavelet-based watermarking into 3 main groups depending on the subbands used for embedding the wavelet. They are 1) methods that use only the lowest frequency (LL) subband [1, 2], 2) methods that use only high frequency subbands [3, 4] and 3) methods that use all wavelet subbands [5, 6]. We discuss an example from each category in below sections.

#### 3.1. Method 1: LL subband based watermarking

A blind watermarking scheme in this category is presented in [1] by etching a signature or a bit sequence in the wavelet domain. In this method, a non-overlapping  $3 \times 1$  running window is passed through the entire LL subband of the wavelet decomposed image. At each sliding position, a rank order sorting is performed on the coefficients  $C_1, C_2$  and  $C_3$  to obtain an ordered list  $C_1 < C_2 < C_3$ . The median value  $C_2$  is modified to obtain  $C'_2$  as follows:

$$C'_2 = f(\alpha, C_1, C_3, w), \quad (11)$$

where  $w$  is a sample from the watermark  $W$  and  $f()$  denotes a non-linear transformation.

For the extraction of watermark bit sequence, the DWT is performed on the received image. Then a rank order sorting is performed with a  $3 \times 1$  running window to obtain sorted elements  $C_1, C_2$  and  $C_3$  at each position. The watermarked bit associated with the particular window position is extracted as follows:

$$w = \arg \min_{w \in (0,1)} |C_2 - f(\alpha, C_1, C_3, w)|, \quad (12)$$

where  $f()$  is the same as mentioned earlier. The extracted watermark is then authenticated by calculating the Hamming distance  $d$  between the original ( $W$ ) and the extracted ( $W'$ ) watermark as follows:

$$d(W, W') = \frac{1}{N_w} \sum_{i=1}^{N_w} W_i \oplus W'_i, \quad (13)$$

where  $N_w$  is the length of the sequence and  $\oplus$  represents the XOR operation between the respective bits.

#### 3.2. Method 2: LH, HL and HH subbands based watermarking

An example of this group is proposed in [3]. After the DWT, the watermark is embedded to the High frequency subbands

as follows:

$$C'_{m,n} = C_{m,n} + \alpha C_{m,n}^2 W_{m,n}, \quad (14)$$

where  $C_{m,n}$  and  $C'_{m,n}$  are the original and modified coefficients, respectively and  $\alpha$  is the parameter which controls the level of watermark,  $W_{m,n}$ .

The watermark detection process requires the watermarked as well as the original image. The DWT is applied to both the original and the received images. Then initially only the difference in  $HH$  in the first decomposition level (the highest frequency subband) is compared for watermark detection. The similarity measure,  $s$ , shown in Eq. (15), is then performed between the difference and the original watermark.

$$s(W, W') = \frac{W \cdot W'}{\sqrt{W' \cdot W'}} / \frac{W \cdot W}{\sqrt{W \cdot W}} \times 100, \quad (15)$$

where  $W$  and  $W'$  are the original and the extracted watermarks, respectively. If the similarity measure is more than a specified threshold, the watermark is deemed to be detected. Otherwise the same procedure is followed with  $HH$  and  $HL$  subband combination or  $HH$ ,  $HL$  and  $LH$  combination *etc.*

#### 3.3. Method 3: All subbands based watermarking

We chose the wavelet based level adaptive thresholding algorithm proposed in [5] as an example to this category. In this case, the length of the watermark vector depends on the number of available significant coefficients which are determined by level adaptive thresholding. For watermark embedding the DWT is performed and the significant coefficients are detected by comparing to the threshold, which is computed as follows:

$$T_i = 2^{\lfloor \log_2 C_i \rfloor - 1}, \quad (16)$$

where  $T_i$  and  $C_i$  denote the threshold value and the largest coefficient at the  $i^{th}$  decomposition level, respectively. The watermark is embedded to the selected coefficients as follows:

$$C'_{m,n} = C_{m,n} + \alpha C_{m,n} W_{m,n}, \quad (17)$$

where  $C_{m,n}$  denotes the chosen significant coefficients is the selected wavelet coefficient,  $W_{m,n}$  is the watermark and  $\alpha$  is the scale factor which is adjusted according to the subband decomposition level. For the watermark detection purpose a similarity test as in Eq. (15) is carried out.

## 4. SIMULATION RESULTS

We evaluate the performance of M-Haar and M-QC wavelets and compare with that of Haar and the D4 wavelets. We report both embedding and the robustness to content adaptation performance. We have used the images from the Kodak image set and commonly used test images Lenna and Mandril.

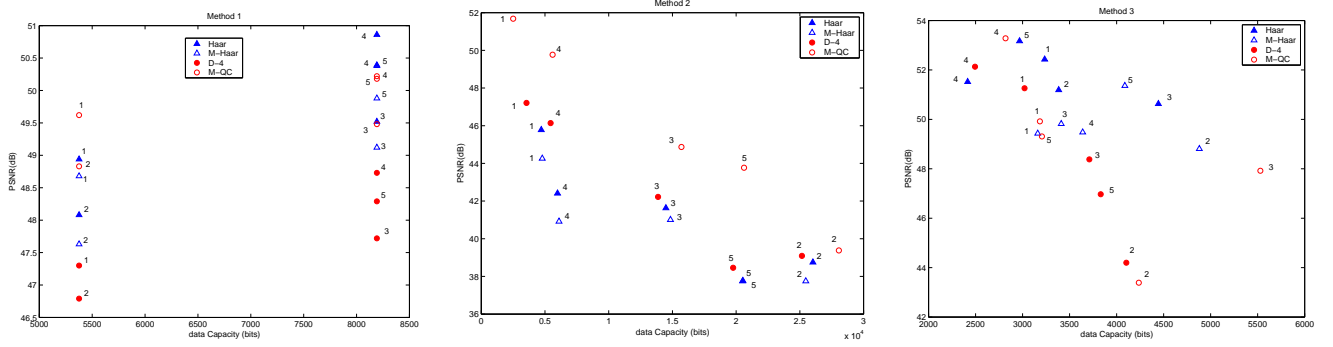


**Fig. 2.** Capacity-distortion plots. Numbers 1 to 5 represent the five images, Lenna, Mandril, Boat, Girl, and House, respectively (the last 3 are from the Kodak image set)

#### 4.1. Embedding performance

In all cases, the DWT is applied on images to 2 decomposition levels, then the watermark is embedded in frequency domain and the inverse DWT is applied to get the watermarked image. We measured the data capacity of the watermark and the imperceptibility of the watermark and show in Fig. 2. The latter was measured using the distortion added by watermark on the original image. It is evident from the plots that the Morphological wavelets result in capacity distortion performance comparable to that of orthogonal wavelets.

#### 4.2. Robustness against content adaptation attack

We compressed the watermarked images using the JPEG2000 (Kakadu v.2.2 implementation available with [18]) to a high quality at full resolution. Then we modelled several content adaptation attacks by extracting new bit streams for full, half quarter resolutions at different bit rates and then decoding to obtain images with different qualities and resolutions.

The resolution adaptation makes the image size smaller than the original size and hence it needs to be up-sized for the cases where higher frequency bands are used for embedding. We resized the adapted image using 3 steps. Firstly, we create a matrix of zeros which has the same size of the original image and then scaled image is included in the top left corner of the matrix. Secondly, an appropriate scaling ( $\times 2$  for half resolution and  $\times 4$  for quarter resolution) is performed. Finally, the 1 level (for half resolution) or 2 level (quarter resolution) inverse DWT is performed using the same wavelet kernel used in watermark embedding.

The detection performances (Hamming distance for Method 1 and similarity measure for Methods 2 and 3) for different compression ratios and resolutions are shown in Fig. 3. A smaller Hamming distance or a higher similarity percentage yields better detection performance. We compare the performance of M-Haar and Q-MC with Haar and D-4, respectively. Morphological wavelets show better detection performances for half and quarter resolutions and at high compression ra-

tios, when compared to the corresponding orthogonal wavelets of the same filter lengths.

### 5. CONCLUSIONS

In this paper, we have discussed the use of Morphological wavelets for wavelet domain watermarking. We have shown how to design non-separable 2D morphological Haar and median based wavelets on quincunx sampling. We analysed the performance by considering various methods of embedding based on the choice of subbands used for embedding. Morphological wavelets show capacity distortion performance comparable with that of orthogonal wavelets. They also show high robustness against resolution and quality scalability in content adaptation attacks.

### 6. REFERENCES

- [1] L. Xie and G. R. Arce, "Joint wavelet compression and authentication watermarking," in *Proc. IEEE ICIP*, 1998, vol. 2, pp. 427–431.
- [2] H. Inoue, A. Miyazaki, A. Yamamoto, and T. Katsura, "A digital watermark based on the wavelet transform and its robustness on image compression," in *Proc. IEEE ICIP*, 1998, vol. 2, pp. 391–395.
- [3] X. Xia, C. G. Boncelet, and G. R. Arce, "Wavelet transform based watermark for digital images," *Optic Express*, vol. 3, pp. 497–511, Dec. 1998.
- [4] M. Hsieh, D. Tseng, and Y. Huang, "Hiding digital watermarks using multiresolution wavelet transform," *IEEE Trans. on Indust. Elect.*, vol. 48, pp. 875–882, Oct. 2001.
- [5] J. R. Kim and Y. S. Moon, "A robust wavelet-based digital watermarking using level-adaptive thresholding," in *Proc. IEEE ICIP*, 1999, vol. 2, pp. 226–230.
- [6] Y. Seo, M. Kim, H. Park, H. Jung, H. Chung, Y. Huh, and J. Lee, "A secure watermarking for jpeg-2000," in *Proc. IEEE ICIP*, 2001, vol. 2, pp. 530–533.
- [7] P. Su, H. M. Wang, and C. J. Kuo, "An integrated approach to image watermarking and jpeg-2000 compression," *J. VLSI Signal Processing*, vol. 27, pp. 35–53, Jan. 2001.
- [8] Y. Fang, N. Bi, D. Huang, and J. Huang, "The m-band wavelets in image watermarking," in *Proc. IEEE ICIP*, 2005, vol. 1, pp. 245–248.

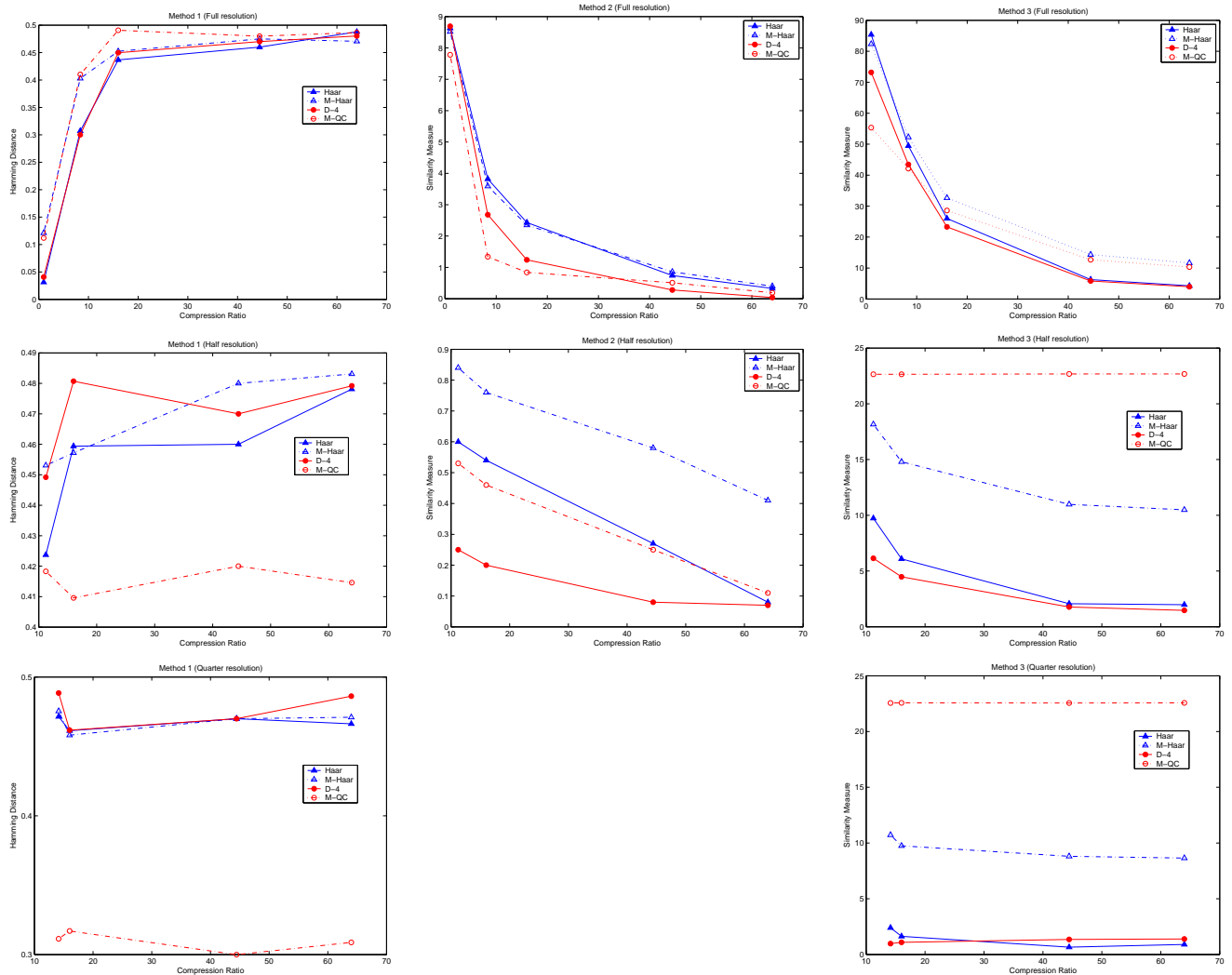


**Fig. 3.** Watermark detection measurements under content adaptation attacks. *Row 1:* Full resolution, *Row 2:* Half resolution and *Row 3:* Quarter resolution. *Column 1:* Method 1, *Column 2:* Method 2 and *Column 3:* Method 3. Watermark cannot be detected at quarter resolution for Method 2 as only the high frequency subbands from a 2-level decomposition are used in watermarking

- [9] A. Bouridane L. Ghouti and S. Boussakta, “High capacity watermarking using balance multiwavelet transforms,” in *Proc. IEEE ICIP*, 2005, vol. 1, pp. 977–980.
- [10] P. Meerwald and A. Uhl, “A survey of wavelet-domain watermarking algorithms,” in *Proc. SPIE Security and Watermarking of Multimedia Contents III*, 2001, vol. 4314, pp. 505–516.
- [11] I. Daubechies and W. Sweldens, “Factoring wavelet transforms into lifting steps,” *J. Fourier Anal. Appl.*, vol. 4, no. 3, pp. 245–267, 1998.
- [12] R. Claypoole, G. Davies, W. Sweldens, and R. Baraniuk, “Non-linear wavelet transforms for image coding using lifting,” in *31st Asilomar Conf. on Signals, Systems and Computers*, 1998, vol. 1, pp. 662–667.
- [13] B. Pesquet-Popescu, H. Heijmans, G. C. K. Abhayaratne, and G. Piella, “Quantisation of adptive 2D wavelet decompositions,” in *Proc. IEEE ICIP*, 2003, vol. 3, pp. 209–212.
- [14] G. C. K. Abhayaratne, “Wavelet filter banks with a 2D spatially adaptive low pass filter for scalable image coding,” in *Proc. Picture Coding Symp.*, 2004, pp. 565–570.
- [15] H. Heijmans and J. Goutsias, “Nonlinear multiresolution signal decomposition schemes: Part II: Morphological wavelets,” *IEEE Trans. Image Processing*, vol. 9, no. 11, pp. 1897–1913, Nov. 2000.
- [16] F. J. Hampson and J.-C. Pesquet, “A nonlinear subband decomposition with perfect reconstruction,” in *Proc. IEEE ICASSP*, 1996, vol. 3, pp. 1523–1526.
- [17] G. C. K. Abhayaratne and H. Heijmans, “A novel morphological subband decomposition scheme for 2D-t wavelet video coding,” in *Proc. Int’l Symp. on Image and Signal Processing and Analysis*, 2003, vol. 1, pp. 239–244.
- [18] D. S. Taubman and M. W. Marcellin, *JPEG2000 Image Compression Fundamentals, Standards and Practice*, Springer, USA, 2002.